Characterization of the flow field in a stepped spillway by PIV

by

A. Amador[(1)], G. Van der Graaf[(2)], M. Sánchez-Juny[(1)], J.Dolz[(1)], F. Sánchez-Tembleque [(3)], J. Puertas [(3)].

[(1)] Universitat Politécnica de Catalunya. Hydraulic, Maritime and Environmental Engineering. Department.

Calle Jordi Girona 1-3. Building D1, 08034 Barcelona, Spain. E-mail: antonio.amador@upc.es.

[(2)] E-mail: gerber.van.der.graaf@aaupc.upcnet.es

[(3)] Centro de Innovación Tecnoloxica en Edificacion e Enxeneria Civil. Universidad de A Coruña.

Campus Elviña, s/n 15192, La Coruña, Spain. E-mail: citeec@udc.es

ABSTRACT

An experimental study was conducted on a large model of a stepped spillway. The particle image velocimetry technique is used to provide the characterization of the flow field in the non-aerated region of the skimming flow regime. The region upstream and next to the inception point of air entrainment is considered critical for evaluation of the cavitation risk in the spillway. Typical flow phenomena like turbulence intensities and shear strain rates in the cavity of the steps, in the shear layer and in the main flow are described. These experimental results give insight in the flow behaviour that cause possible cavitation inception.

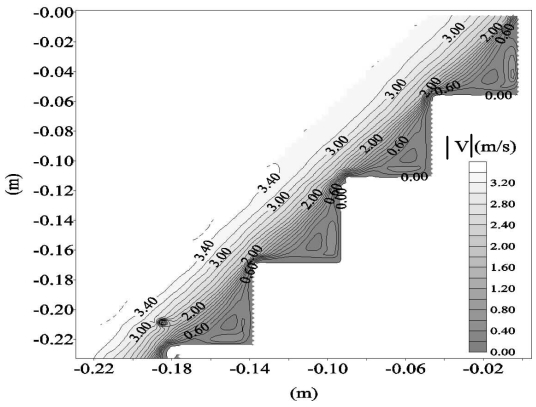

Fig.1. Mean velocity field in skimming flow in a stepped spillway (q=0.11 m^2/s).

1. INTRODUCTION

Stepped spillways are hydraulic structures that have regained significant interest for researchers and dam engineers in the last two decades, specially due to technological advances in construction of roller compacted concrete (RCC) dams (Chamani and Rajaratnam, 1999; Pegram et al. 1999; Sánchez-Juny, 2001; Boes and Hager, 2003). The concrete placement in lifts allows a fast construction of spillway steps on the downstream dam faces. The other advantage, besides the construction economy, is the higher energy dissipation along the chute in comparison with a conventional smooth spillway that leads to a reduction of the stilling basin dimensions at the end of the spillway (Matos, 2000). For high flow rates (q=15-20 m^2/s) possible damages on the structure may be caused by the dynamic loads induced by the flow. Mainly cavitation effects are believed to be the cause of these damages. Therefore, a better insight in the complex flow behaviour is needed in order to optimize the design of these stepped spillways.

Two kinds of flow regimes occur on stepped spillways: the nappe flow at low flow rates and skimming flow. The first flow regime is characterized by a series of overfalls, with the water plunging from one step to another. In skimming flow the water flows as a coherent stream down the pseudo-bottom formed by the outer edges of the steps, intense cavity recirculation is then observed in the zone delimited by the pseudo-bottom and the step faces. For typical design discharges of stepped spillways over RCC dams, skimming flow is usually found (Essery and Horner, 1978; Sánchez-Juny, 2001; Chanson, 2002). This paper deals with skimming flow regime.

At the upstream region of the chute the free surface is smooth and glassy and no air entrainment occurs, however the presence of the steps enhance the flow turbulence and hence the growth of the boundary layer. The starting point of air entrainment (inception point) is defined by the location where the thickness of the boundary layer equals the flow depth. Downstream of the inception point, rapid free surface aeration is observed. The existence of sufficient air content near the solid boundaries prevents cavitation damage. Special attention was devoted to the non-aerated region of the spillway, considered critical for evaluation of cavitation risk in the structure.

An experimental study was conducted on a large model flume using particle image velocimetry instrumentation. The use of this non-intrusive technique aimed at improving the understanding of the flow field characterization in stepped spillways, in particular obtaining new information about the internal flow features that fill the cavities between the main flow and the faces of the steps.

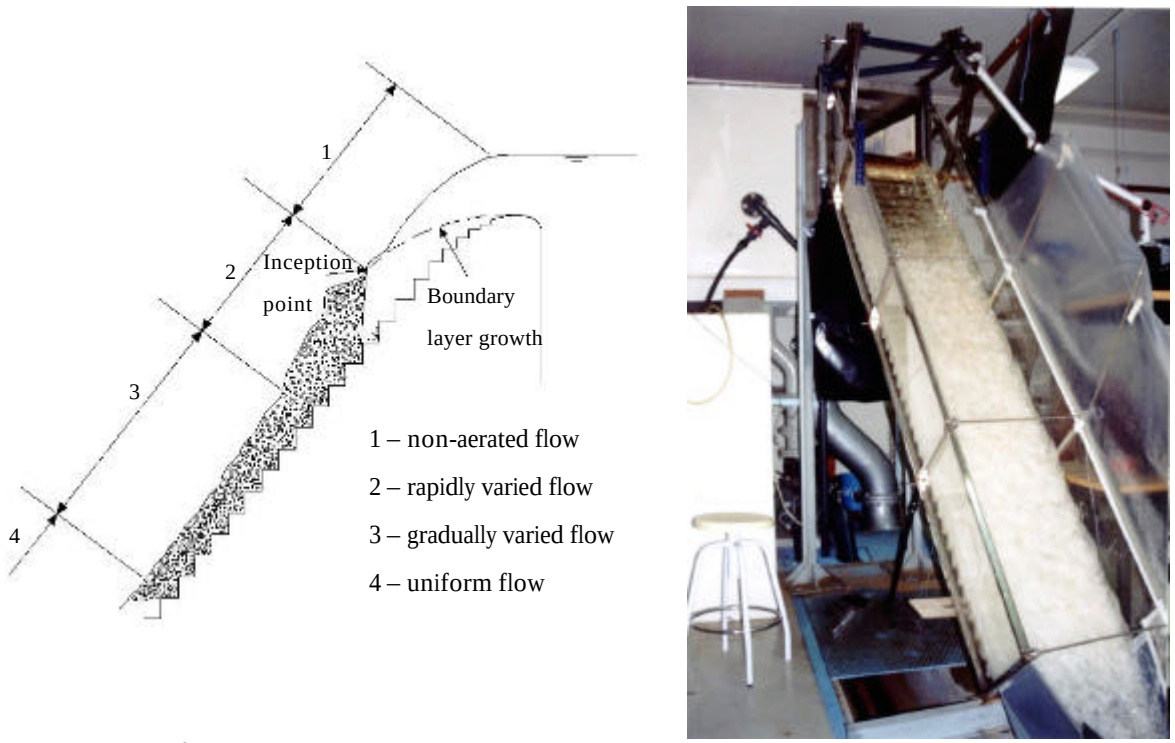

Fig. 2. Skimming flow regime in a stepped spillway.

2. EXPERIMENTAL SETUP

2.1 Stepped spillway

The experiments were conducted on a large model flume of width 0.50m and height 2.0m, with step height of 0.05 m and bottom inclination of 51.3º corresponding to a slope (V:H) of 1:0.8. The pseudo-bottom, formed by the imaginary line joining the step edges, was used as the reference level for the flow depths. The side walls as well as the steps are made of transparent methacrylate to realize optical access from all directions. The tests were performed for a unit flow discharge of 0.11 m^2/s. Based on the flow depth, the Reynolds number was then 1.1×10^5. The flow has been observed at four different steps in the non-aerated flow region of the spillway. The outer edge of the steps are located at a distance (L) from the spillway crest of 0.599 m (step1), 0.663 m (step2), 0.727 m (step3), 0.791 m(step4).

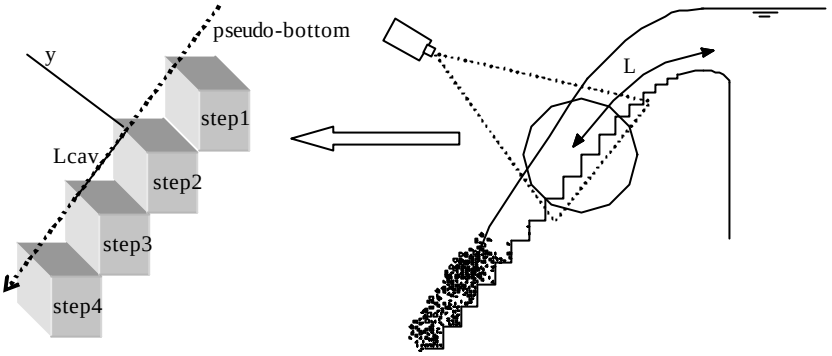

Fig. 3. Schematic view of the observed area of study and notation used.

2.2 PIV system

The PIV system is composed by a double-pulsed Nd-Yag laser, with a energy of 400 mJ per pulse, a 1024×1280 pixel resolution, high sensitive peltier cooled, CCD camera. A Nikkor 50mm 2.8, together with a narrow bandwidth filter that passes the 532 nm light from the Nd-Yag laser, is mounted on the CCD camera. An electronic sequencer synchronizes the camera and laser pulses.

The water was seeded with 70 μm ceramic micro spheres. The images only covered two steps, as bigger measurement areas implied unacceptable perspective errors. The flow has been observed separately at two different positions that are partly overlapping. Afterwards, the PIV data sets observed from these positions have been composed together (covering four steps) for statiscal analyses. The camera captured double frame double exposure particle images. The separation time was adjusted at 250 μs between two laser pulses in order to give maximum particle image displacement of eight pixels.

The images are interrogated by a self-written algorithm resulting into estimators of the particle image displacements on a rectangular grid. Therefore, pair of two image frames are recorded with the specified time delay. Both image frames are subdivided into small interrogation area's that are adjacent or overlapping. Interrogation area's at identical positions in the image frames are correlated by means of Fast Fourier Transformation. The FFTW library (Frigo, 1998) has been used for this purpose. This library allows Discrete Fourier Transforming of interrogation area's of arbitrary dimensions at competitive high calculation speeds. From the two-dimensional cross-correlation function the position of the highest peak, representing the mean, or most probable, displacement of the particle images, is estimated. In order to obtain high-accuracy estimators of the particle displacements, the correlation peak position is calculated at sub-pixel level by the three-point Gauss interpolation scheme.

The accuracy and reliability of the resulting PIV estimators have been examined by validation tests on synthetic, computer generated images as well as on physical images. These tests show that the maximum rms in the estimators is

lower than 0.1 pixel, meaning an accuracy in the measured velocities of 52mm/s for the experiments discussed in this paper.

Zero offsetting is applied in order to optimize the signal and to minimize biasing effects in the PIV estimators (Westerweel et al., 1997). The interrogation of the images initiates with large dimensions of the interrogation area's that are reduced in size after each interrogation. In this way, high dynamic velocity ranges are obtained in combination with a high spatial resolution. A central differential interrogation scheme is used to improve the accuracy of the estimators, especially in regions of rotational flows. This is obtained by shifting the interrogation area of the first image by half the magnitude of the PIV estimator in backward direction and the interrogation area of the second frame in forward direction (Werely and Meinhart, 2001). For this study, adaptive interrogation area sizes have been used from 64×64 pixels to 48×48 pixels, with an overlapping of 50 percent (i.e. 24 pixels). The resulting PIV estimators are examined on the velocity gradient. A maximum gradient of three pixels within the interrogation area (i.e. approximately the particle image diameter) is chosen as a criterium for acceptance. Some relevant data sets of each experiment are checked on peak-locking effects by examining the statistics of the PIV estimators at sub-pixel level. All data are validated on outliers by the median test. Detected outliers are substituted by the local mean value of its neighbouring estimators. The detection threshold for acceptance of outliers is obtained from an estimation of the data yield (determined by the image density i.e. particle concentration) and from the residue statistics of the estimated velocity field (Westerweel, 1994; Keane and Adrian, 1990).

The algorithm to interrogate the images, validate and post-process the PIV data, has been implemented as a set of command-line driven programs (Gpivtools) for quick, non-graphic and non-interactive processing and as a Graphic User Interface program (Gpiv) as well. Gpiv allows visualizing each image-pair, together with PIV estimators and its derivatives in a single display, while the parameter settings and processes are controlled from a console interface. Some graphical output, like correlation function and histograms may also be displayed in the console. The code has been issued under the GNU Open Source Licence and is available at: http://gpiv.sourceforge.net.

3. RESULTS AND DISCUSSION

3.1 Effect of sample size on ensemble averaged PIV data

To obtain a proper estimation of the mean flow and turbulence statistics from the velocity fields, the data are examined on statistical independency and on sample length. Statistical independency has been investigated by calculating the correlation of the velocities at a specific location in the flow $Rv_x(dt)$ and $Rv_y(dt)$. Therefore, a location in the main flow, shear layer and within the step cavity has been observed. A total number of 500 velocity fields have been recorded with separation time of one second. For all three locations no velocity correlation is found already after a time delay of one second. Only some noise in the correlation is observed that stay below 0.1.

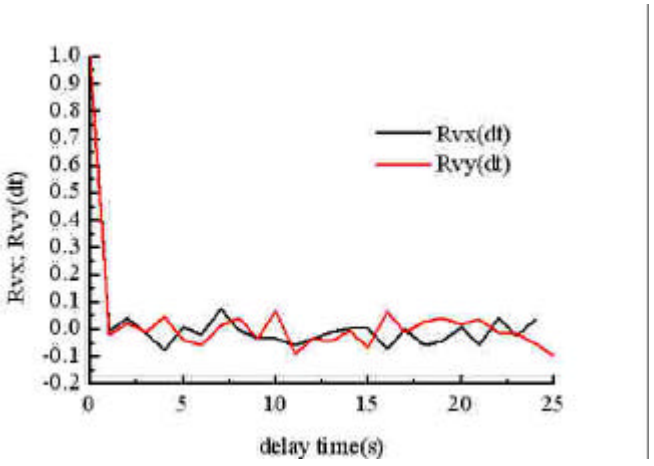

Fig. 4. Velocity correlations in the shear layer, $Rv_x(dt)$ and $Rv_y(dt)$ versus delay time .

The sample length (i.e. the total number of velocity fields) are tested on convergence of the mean and variance in the velocities. Therefore, the mean and Rms of the absolute velocity have been regarded. Figure 5 shows a convergence of the estimated mean towards a constant value. For sample length of more than 200, the estimators hardly change for the main flow and shear layer. In case of the flow within the step cavity, minor changes are found for sample lengths larger than 300. Similar results are found in the estimators of the Rms of the velocities.

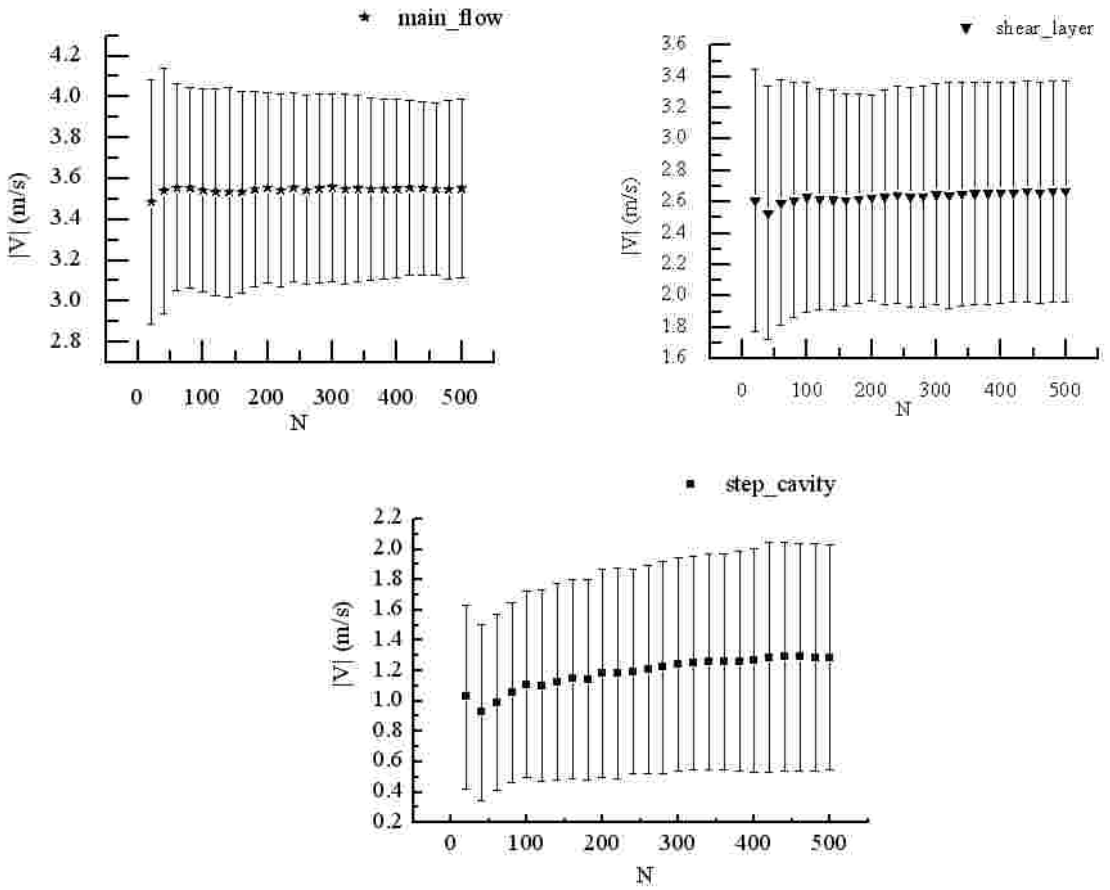

Fig. 5. Mean and Rms (half the length of the error bar) of absolute velocity versus sample length (N).

3.2 Velocity field

The detailed contour maps of the mean absolute velocity (|V|) and root mean square of the velocity fluctuations (Rms) obtained from 500 PIV realizations are shown in figure 6. The velocity vector spacing is 3.0 mm (i.e. 24 pixels) and kriging interpolation was chosen as gridding method.

From the mean velocity magnitude plot, it can be observed that the flow is accelerating and developing in the downstream direction. The free stream velocity (V_{max}) varies from 3.2 m/s to 3.6 m/s. A well defined recirculation zone occupies part of the steps cavities, these quasi-steady rollers are maintained through the transmission of shear stress from the overlying flow. Considering the recirculatory motion a solid body rotation for an equivalent circumference trajectory of 2 cm diameter, the angular velocity and frequency of rotation were estimated to be approximately 40-50 $rads^{-1}$ and 6-8 Hz in the four steps studied. The shear layer separates from the upstream outer step edges and impinges at the downstream part of the horizontal face of the step.

In relation to the root mean square contour map, there is a gradual increase in the streamwise direction of the Rms values at the outer region (nearer to the free surface) of the main flow. Nevertheless the highest Rms values are situated near the pseudo-bottom (imaginary line joining two adjacent step edges) where maximum turbulent momentum transfer occurs between the main flow and the cavity flow.

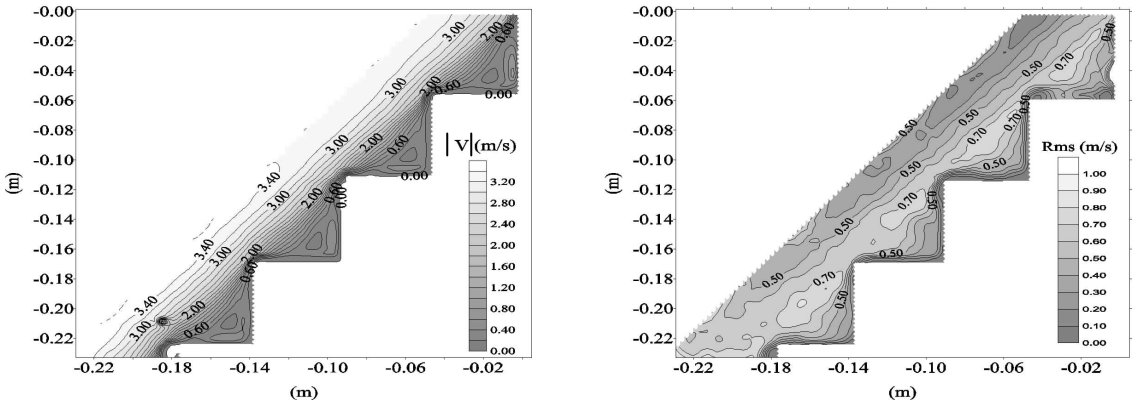

Fig. 6. Mean absolute velocity and root mean square contour maps ($q=0.11m^2/s$).

In this study, mean velocity profiles normal to the pseudo-bottom were taken at different positions along the step cavity length, Lcav (see figure 3). The velocity distribution at the step edges can be approximated by a power law:

$$\frac{V}{V_{\max}} = \left(\frac{y}{d}\right)^{1/N} \tag{1}$$

where V is the velocity in the streamwise direction, V_{max} is the free stream velocity and δ is the boundary layer thickness defined as the perpendicular distance from the pseudo bottom to where the velocity is 99% of its maximum value. The exponent N determined for the upstream edges of step 2 and 4, was 3.4 in close agreement with the value of 3.3 obtained by Matos (1999) using a flushed Pitot tube in a similar model of a stepped spillway. In conventional smooth spillways the value of N=6.0 from the analysis of Cain (1978) and Chanson (1989), is usually suggested for the developing boundary layer upstream of the inception point. This comparison indicates that the mean velocity profile rises much more steeply from the reference level (y=0) in smooth spillways than in stepped spillways and then it is flatter away from the "bottom".

Between the step edges (0<x<Lcav), the velocity gradients at the upstream part of the cavity (0.25 Lcav) are steep, but weakens towards the reattachment point in downstream face of the step (0.50Lcav, 0.75Lcav), this suggests a local developing shear layer emanating from the step edge, like was recently shown by Gonzalez and Chanson (2004). In the recirculation region, the maximum reverse flow velocities found are 0.11-0.12V_{max} (step 2 and 4 respectively) and are located near the step surfaces.

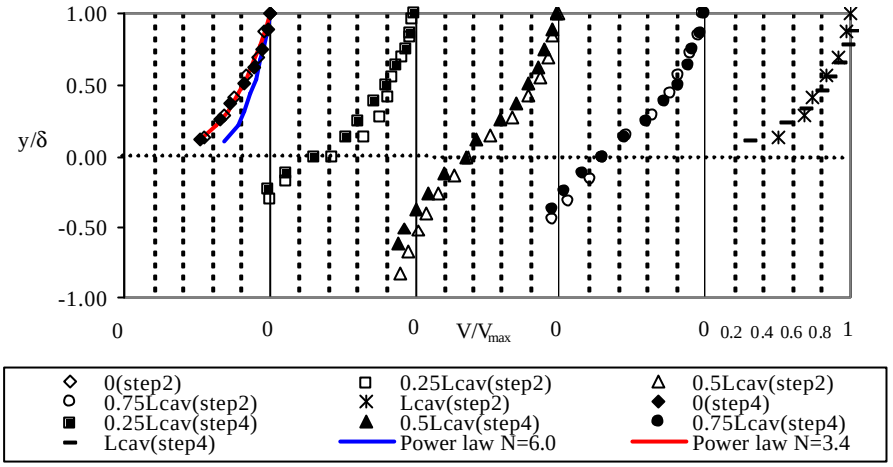

Fig. 7. Mean velocity profiles normal to pseudo-bottom, along the steps cavities (Lcav).

The turbulence intensity, defined as the ratio of the root mean square velocity fluctuations by the local mean velocity (Rms(v)/V), distributions along the step cavity are presented in figure 8.

Above the pseudo-bottom, a decrease of the turbulence intensities towards the free surface is observed, the flow is accelerating and the turbulence is suppressed in the water surface direction. Near the pseudo bottom in the zone of the separated shear layer, the Rms/V reach values comprised between 55-70%. These velocity fluctuations are much higher than the existent in boundary layers over smooth open channels , Rms/V=20%, (Nezu and Nakagawa, 1993). The increase in the magnitudes of flow turbulence will cause greater pressure fluctuations over the boundary surfaces than the usually found in conventional smooth spillways.

In the zone of the reverse flow, the large turbulence intensities found can be explained by the high unsteadiness imposed by the turbulent shear layer.

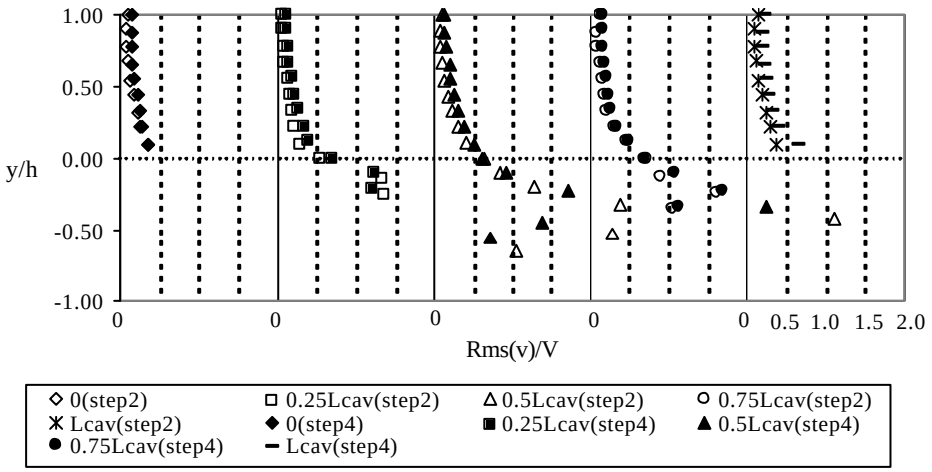

Fig. 8. Turbulence intensity (Rms(v)/V) distributions, along the steps cavities (Lcav).

3.3 Vorticity and shear strain fields

The average spanwise vorticity (ω_z) and shear strain (ε_{xy}) fields were obtained from the ensemble averaged velocity PIV data. These terms of the deformation tensor are defined as:

$$w_z = \frac{dV_y}{dx} - \frac{dV_x}{dy} \quad (2); \quad e_{xy} = \frac{dV_y}{dx} + \frac{dV_x}{dy} \quad (3);$$

The Richardson extrapolation scheme was employed for estimation of the spatial derivatives of the velocity gradient tensor, this finite differentiation scheme is implemented for data spaced at uniform dx, according:

$$\left(\frac{df}{dx}\right)_i \approx \frac{f_{i-2} - 8f_{i-1} + 8f_{i+1} - f_{i+2}}{12\Delta X} \quad (4)$$

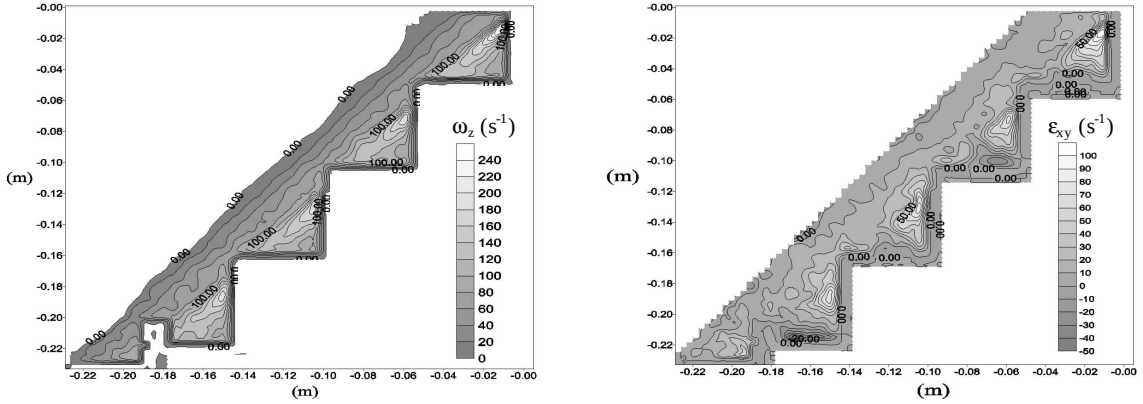

Fig. 9. Mean vorticity (w_z) and shear strain (e_{xy}) fields (q=0.11 m^2/s).

The contour plots given in figure 9, show the highest levels of mean shear strain rate (ε_{xy}) just behind the step edge and are also associated with maximum vorticity (ω_z) values (160 s^{-1}). More downstream, towards the centre of the cavity a gradual decrease of the vorticity, with values between 80 and 100 s^{-1}, is observed. This is in good agreement with the angular velocities (see 3.2) estimated from the mean velocity field for the large recirculation zone, following the Stokes theorem equation.

Assuming valid the turbulent-viscosity hypothesis, the production/generation of turbulent kinetic energy is (Pope, 2000):

$$P = -\langle v_x \cdot v_y \rangle e_{xy} = g_T e_{xy} e_{xy} \quad (5)$$

where $-\langle v_x.v_y \rangle$ is the mean Reynolds shear stress, γ_T is the turbulent viscosity and ε_{xy} the mean shear strain rate. The production is then proportional to the mean shear strain rate. This shows that the zone just behind the step edge is a region of turbulence production/generation and the formation and growth from behind the steps edges of large scale turbulent structures has associated local pressure reductions in the vicinity of vortex cores. Under extreme flow conditions these time dependent flow events can yield the known effect of vortex cavitation inception in hydraulic structures (Baur and Kongeter, 1999).

4. CONCLUSIONS

Particle image velocimetry measurements for a skimming flow regime over a stepped spillway are described. The non aerated flow region near the inception point of the spillway was studied. This region is considered critical for evaluation of the cavitation risk.

In this experimental study significant differences were observed in the mean velocity and turbulence intensity distributions between stepped and smooth spillways. The nature of the spillway surface alters the turbulent energy production process, which reflects in the resulting turbulence characteristics such as the mean velocity and Reynolds stresses (Djenidi et al., 1999).

The mean velocity field revealed the presence of a large recirculation zone inside the step cavity and a separated turbulent shear layer that impacts in the downstream part of the horizontal step faces. The velocity fluctuations described by the root-mean square of the instantaneous velocities showed maximum values near the pseudo-bottom where important momentum transfer occurs between the overlying and cavity flow.

The zone just behind the step edge was identified as a turbulent production flow region. In this zone maximum average vorticity was observed with a gradual decrease towards the centre of the step cavity. The random formation of coherent motions that are convected in the streamwise direction can be considered the responsible for the unsteady pressure fluctuations that under extreme flow conditions would cause cavitation inception in stepped spillways.

ACKNOWLEDGEMENTS

The first author acknowledges the financial support of the Fundação para a Ciência e Tecnologia (Portugal, Praxis XXI, BD/3056/2000).

REFERENCES

Baur, T. and Kongeter, J. “PIV with high temporal resolution for the determination of local pressure reductions from coherent turbulence phenomena” Proc. 3rd International Workshop on Particle Image Velocimetry, University of California, Santa Barbara, 1999.

Boes, R. and Hager, W. “Two Phase flow characteristics of stepped spillways”. Journal of Hydraulic Engineering, Vol.129 Nº9 :661-670, 2003.

Cain, P. “Measurements within self-aerated flow on a large spillway” Phd thesis, University of Canteboury, Christchurch, New Zealand, 1978.

Chamani, M. and Rajaratnam N. “Characteristics of skimming flow over stepped spillways”. Journal of Hydraulic Engineering, Vol. 125, Nº4: 361-368, 1999.

Chanson, H. “ Flow downstream of an aerator. Aerator spacing”. Journal of Hydraulic Research, Vol. 27, Nº4: 519-536, 1989.

Chanson, H. “The hydraulics of stepped chutes and spillways”. Ed. A.A. Balkema - Rotterdam, 2002.

Djenidi, L.; Elavarasan R. and Antonia, R. “ The turbulent boundary layer over transverse square cavities”. Journal of Fluid Mechanics, Vol. 395: 271-294, 1999.

Essery, I. and Horner, M. “The hydraulic design of stepped spillways”. Ciria Report nº33. 1978.

Frigo, M. and Johnson, S.G. “FFTW: An adaptive software architecture for the FFT”, ICASSP conference proceedings, 3, 1381-1384, 1998.

Gonzalez, C. and Chanson, H. “Interactions between cavity flow and main stream skimming flows: an experimental study”. Canadian.J.Civil Engineering. Nº 31: 33-44, 2004.

Keane, R. and Adrian, R. “Optimization of particle image velocimeters part 1: double pulsed systems”. Meas. Science Technology, 1:1202-1215, 1990.

Matos, J. “Hydraulic design of stepped spillways over RCC dams”. Proc. of Intern. Workshop on Hydraulics of stepped spillways, Zurich, Ed. Balkema, Rotterdam: 187-194, 2000.

Nezu, I. and Nakagawa, H. “ Turbulence in open channel flows”. IAHR Monograph series, Ed. Balkema, Rotterdam, 1993.

Pegram, G.; Officer, A. and Mottram S. “ Hydraulics of skimming flow on modeled stepped spillways”. Journal of Hydraulic Engineering. Vol. 125, Nº 5: 500-510, 1999.

Pope, S. “Turbulent flows”. Ed. Cambridge University press, 2000.

Sánchez-Juny, M. “Comportamiento hidráulico de los aliviaderos escalonados en presas de hormigón compactado. Análisis del campo de presiones”. Phd thesis, Universitat Politécnica de Catalunya, Barcelona, 2001.

Werely, S and Meinhart, C. “Second-order accurate particle image velocimetry.” Experiments in Fluids, 31: 258-268, 2001.

Westerweel, J. “Efficient detection of spurious vectors in particle image velocimetry data”. Experiments in Fluids, 16:236-247, 1994.

Westerweel, J., Dabiri, D., Gharib, M. “The effect of a discrete window offset on the accuracy of the cross-correlation analysis of digital piv recordings.” Experiments in Fluids, 23: 20-28, 1997.